SCALING METHODS IN SOIL PHYSICS

Edited by

Yakov Pachepsky
David E. Radcliffe
H. Magdi Selim

CRC PRESS

Boca Raton London New York Washington, D.C.

15 Application of a Neural Network-Based Spatial Disaggregation Scheme for Addressing Scaling of Soil Moisture

T.D. Tsegaye, W.L. Crosson, C.A. Laymon, M.P. Schamschula, and A.B. Johnson

CONTENTS

I. INTRODUCTION

Soil moisture plays an important role in the near-surface meteorology, locally as well as globally, by regulating the surface–atmosphere energy exchange. Variation of soil moisture directly affects plant growth and crop yields. Most researchers in soil science, hydrology, meteorology, and remote sensing seek better quantification of soil moisture variation, in time and in space, in order to improve model performance. Thus, improving the techniques to estimate soil moisture on a local and regional scale is the main focus of recent research efforts in hydrology[1] and microwave remote sensing of soil moisture.[2–5]

0-8493-1374-0/03/$0.00+$1.50

Soil properties differ widely in type and distribution.[6] This variation, in turn, causes large differences in the way dissimilar soil types store and transmit water, and dictates the need for hydrologic investigations on projects such as those required to relate remotely sensed data to surface and subsurface hydrology. Hydrological prediction at the micro- and mesoscales is intimately dependent on the ability to characterize the spatial variability of soil hydraulic properties.

Several soil and plant properties are needed for modeling surface and subsurface phenomena.[7–9] The lack of these data at the required spatial resolution is the greatest impediment to the successful application of local and regional scale hydrology models.

Soil scientists and hydrologists are well aware of the nature of spatial variability in hydraulic properties. Saturated hydraulic conductivity of a single soil sample may vary considerably.[6] There is even greater variability of soil hydraulic properties among samples of different soil textures. Soil hydraulic properties are generally observed in the field over a wide range of scales from a few centimeters to kilometers, depending on the intended use. Characterizing and understanding these properties is important for improved performance of local and regional scale hydrology models and accurate estimation of the distribution of soil moisture in space and time.[7]

II. STATEMENT OF PROBLEM

Estimation of surface soil moisture using microwave remote sensors holds great promise for many applications, including numerical weather prediction and agriculture. However, there exists a scale disparity between the resolutions of future satellite-borne microwave remote sensors (30 to 60 km) and the much finer scales at which soil moisture estimates are desired (~1 km). Hydrology models may be useful for bridging this gap, as the factors controlling soil moisture variability (precipitation, soil and vegetation properties, terrain slope) are known with reasonable accuracy at fine spatial scales and can be used in models to estimate the spatial distribution of soil moisture at high resolutions. Therefore, to facilitate the assimilation of remote sensing data, it is important to explore ways to disaggregate low-resolution passive microwave remote sensing data to the higher resolution of a hydrologic model.

III. SCIENTIFIC OBJECTIVE AND APPROACH

In this section we describe tests of the performance of a neural network-based model, called DisaggNet, developed by the authors to disaggregate low-resolution satellite microwave remote sensing data for the purpose of estimating soil moisture at finer scales used in hydrologic models. We also quantify estimation errors as a function of input data resolution. Ideally, the purpose of a disaggregation scheme is to produce the "correct" high-resolution (subpixel) pattern of soil moisture from lower-resolution remotely sensed observations. For several reasons, it is difficult to develop and validate such a scheme.

First, the correct subpixel soil moisture pattern, or ground truth, within a satellite footprint is rarely if ever known within acceptable error bounds. Thus, adequate data for developing statistical models or more complex models such as neural networks, both of which rely on some type of data fitting, do not exist, and may never exist, for areas larger than field scale. When satellite data become available operationally on a global scale, it may be possible to develop a disaggregation scheme using a combination of remotely sensed data and output from coupled hydrology–radiative transfer models (RTM). Currently, however, high-resolution data from aircraft platforms are available for only limited areas and times during intensive field experiments. While these could theoretically be used to develop a disaggregation scheme, the results would likely not be transferable to other geographical areas or even to different hydrometeorological conditions in the same region. Furthermore, the amount of data needed to train a neural network adequately exceeds the amount obtained in a typical field campaign.

Because of this paucity of remotely sensed observations, we believe that the most viable approach is to train a neural network using solely model output, and then test its performance using actual remotely-sensed data. In this scenario, model-simulated data serves as a proxy for satellite-borne microwave remote sensor data. This approach necessitates the following assumptions:

1. The surface hydrology–radiative transfer model accurately simulates the spatial patterns of soil moisture and brightness temperature within an actual or hypothetical low-resolution satellite footprint, although the model estimates averaged over the footprint may be biased with respect to the satellite estimates.
2. Low-resolution brightness temperature observations are unbiased and have a known noise variance with respect to the ground truth at the scale of the observations.
3. The functional relationship between brightness temperature and soil moisture "learned" by the neural network is consistent with the relationship simulated by the RTM. This can be easily verified from the outputs of the neural network and RTM.

Following these assumptions, we designed the neural network to simulate the model (high-resolution) soil moisture pattern within each satellite footprint while preserving the mean remotely sensed brightness temperature (T_B) or microwave emissivity (ε), the main neural network input, which may differ significantly from the model mean over the footprint. To the extent that the emissivity–soil moisture relationship is linear, the neural network will also preserve the footprint-mean soil moisture. The neural network, once trained, will be applicable to a range of hydrometeorological conditions within a geographic domain, but would need to be retrained in order to be transferred to another domain.

Here we present a description of the disaggregation methodology and results related to training and testing of the scheme using solely model data. In future research we will apply the scheme to aircraft remote sensing data as a more relevant and revealing application of the method.

IV. SAMPLING SITE DESCRIPTION

The research was conducted in LWRB in Southwest Oklahoma during the Southern Great Plains 1997 (SGP97) Hydrology Field Experiment. Further detailed description of the experimental plan can be found elsewhere (http://hydrolab.arsusda.gov/sgp97/). The watershed covers 603 km^2 and is a tributary of the Washita River. The climate of this location is classified as moist and subhumid, and the average annual rainfall is approximately 747 mm. In this watershed the summer is typically long, hot, and relatively dry. The average daily high temperature for July is 94°F (35°C), and the average accumulative rainfall for July is 56 mm. The topography of the land is gently to moderately rolling and the average slope within the entire sampling location ranges from 1 to 5%. Additional information about the LWRB can be found in the works of Allen and Naney.[10]

V. SAMPLING LOCATION AND ANALYSIS

To characterize and assess the spatial distribution of soil hydraulic properties in the LWRB, soil core samples were collected from four sites: Apache, Berg, DOE-EF26, and NOAA. Multiple undisturbed soil cores, 3.0-cm length by 7.6-cm diameter, were taken from 5, 15, 30, 50, and 70 cm soil depths using a Uhland core sampler[12] from these sites to characterize the spatial distribution of soil hydraulic properties including hydraulic conductivity (K_{sat}), bulk density, and soil water retention. Using a water content reflectometer, soil moisture measurements were also made at 30-min intervals at ten depths, from 3 to 70 cm to continuously examine the soil moisture distribution for the various soils in the LWRB.

A. Analysis of Soil Physical Properties

Saturated hydraulic conductivity (K_{sat}) was determined by ponding 3.6 cm of water on top of each core under a constant head. A 6- to 8-h equilibration period was allowed, after which preliminary outflow measurements were taken to determine if the rate of outflow was consistent. Outflow was determined for a 15-min period, after which K_{sat} was calculated using Darcy's equation.[11]

Following K_{sat} measurements, soil water retention was determined for each core at matric potential values of 0, –33.3, –100, –500, –1000 and –1500 kPa. A pressure plate apparatus was used to determine soil water retention for all matric potentials. Soil water retention was expressed in terms of volumetric water content using the bulk density of individual cores for the conversion. Bulk density was calculated for each soil core.[12]

VI. MODELS AND DATA

A. Models

1. SHEELS

We have used the land surface flux–hydrology model SHEELS (simulator for hydrology and energy exchange at the land surface), the physics of which are based on the biosphere–atmosphere transfer scheme (BATS) of Dickinson et al.[13] Figure 15.1 depicts the main physical processes simulated in SHEELS. Variables such as surface energy fluxes and temperatures are modeled similarly to an earlier version of the model.[14] Subsurface processes in SHEELS differ significantly from BATS.[15] In SHEELS, the number and depth of soil layers is user defined, permitting higher vertical resolution near the surface where temperature and moisture gradients are large. The soil water dynamics algorithms in SHEELS include Darcy flow to model vertical subsurface fluxes and a kinematic

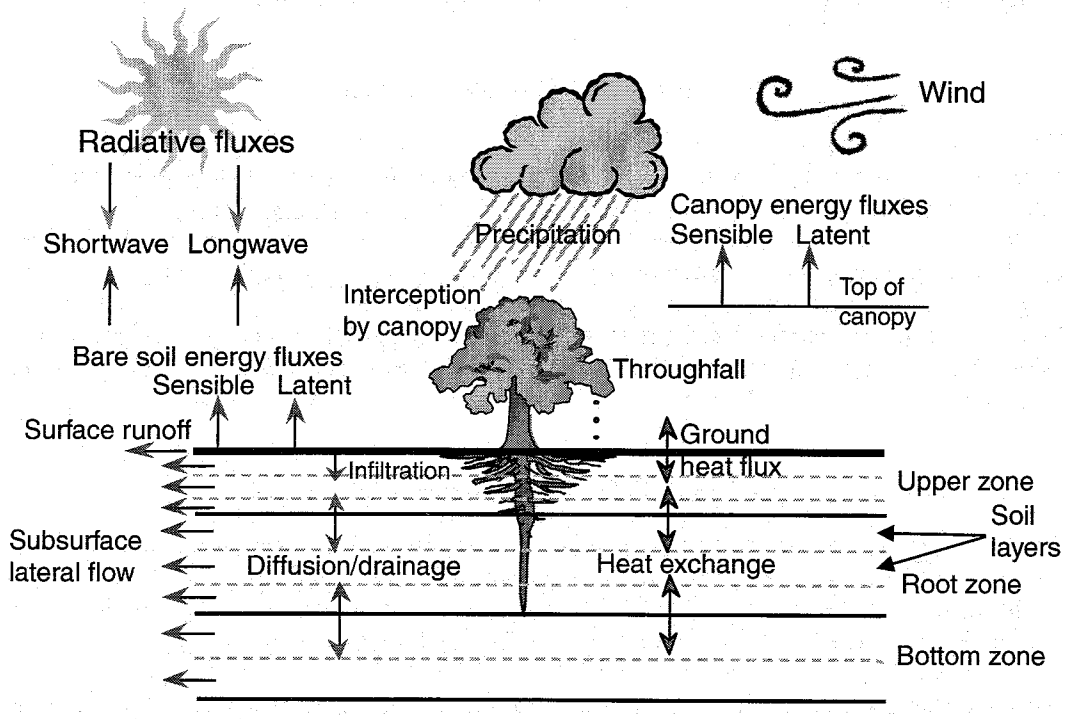

FIGURE 15.1 (See color insert following page 144.) Schematic representation of the basic energy flux and hydrologic processes in the simulator for hydrology and energy exchange at the land surface (SHEELS).

wave approach to simulate overland flow, thus providing a mechanism for estimating the three-dimensional soil water fluxes.

2. Forward Radiative Transfer Model

The forward radiative transfer model coupled with SHEELS is based on the coherent wave model of Njoku and Kong[16] and is used to estimate L-band (1.413 GHz) microwave brightness temperature. The effects of surface roughness and vegetation are corrected for using methods described in Choudhury et al.[17] and Jackson and Schmugge.[18] SHEELS supplies the required RTM inputs of soil moisture and temperature profiles and surface temperature. The remaining input variables (surface roughness, vegetation water content and soil density profiles) are based on measurements. The RTM has been tested and validated with field data.[19]

3. Disaggregation Neural Network (DisaggNet)

We have approached the problem of disaggregation using a linear artificial neural network (ANN). The ANN chosen is the simplest one imaginable, consisting of a single neuron. All of the inputs are weighted and then summed; thus the input to output mapping function is linear. Inputs and outputs of DisaggNet are described in Section III.

B. Model Domain and Data

We applied the disaggregation scheme using data collected across the LWRB in south central Oklahoma (Figure 15.2) during the Southern Great Plains 1997 Hydrology Experiment (SGP '97) conducted during June and July 1997.[20] Aircraft remote sensing brightness temperature data were collected nearly daily by the electronically steered thinned array radiometer (ESTAR) for a region encompassing the LWRB. ESTAR observations are used here only to initialize the surface soil moisture state in SHEELS. We restricted our simulations to the approximate 600-km^2 area of the LWRB because it contains the highest concentration of meteorological and soil moisture measurements in the SGP '97 experimental domain. We have applied the disaggregation scheme for the period from June 18 (day 169) through July 20 (day 201).

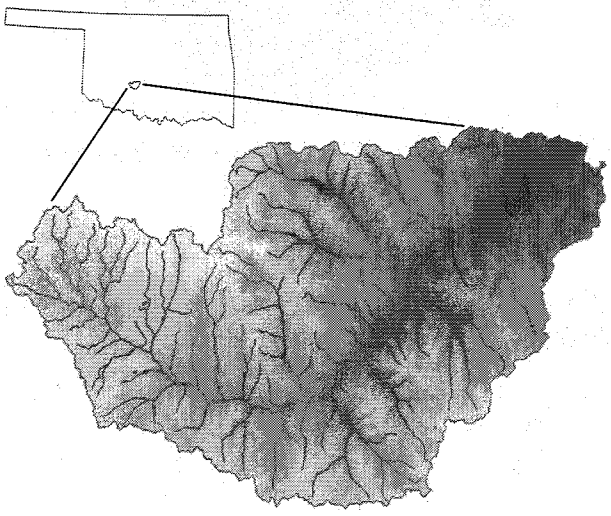

FIGURE 15.2 (See color insert following page 144.) Digital elevation model and stream network for the Little Washita River Basin, Oklahoma.

A model grid of 800 m, coincident with the ESTAR grid, was used in SHEELS simulations. Land surface properties were specified on that grid in SHEELS by the following data sets:

- Elevation, slope: U.S. Dept. of Agriculture/Agricultural Research Service (USDA/ARS) 30 m DEM
- Hydrography: U.S. Geological Survey digital line graphs (DLGs)
- Vegetation parameters: SGP '97 30-m land cover
- Soil properties: CONUS 1-km multilayer soil hydrologic characteristics
- Meteorological and soil moisture and temperature data: Oklahoma Mesonet, USDA/ARS Micronet, SGP '97 soil profile stations
- Precipitation: USDA/ARS Micronet rain gauge data

The raw data having native resolutions finer than 800 m were aggregated to the model grid using the mean value, or in the case of categorical data such as soil and land cover classes, the mode. The CONUS soil properties were resampled from 1 km to the 800-m model grid; surface soil texture classes are shown in Figure 15.3. Meteorological data, with the exception of rainfall, were averaged across all sites and applied uniformly across the LWRB. Distributed rainfall estimates for the model grid were obtained from the Micronet point measurements and converted to 800-m gridded data by constructing Thiessen polygons around each gauge location.

Selected physical properties of the LWRW soils, as sampled during the SGP'97 field hydrology experiment, are presented in Table 15.1. Except for the Apache and Berg sites, bulk

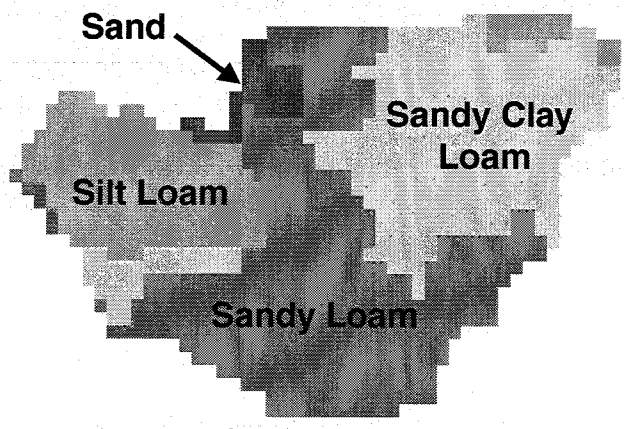

FIGURE 15.3 (See color insert following page 144.) Surface soil texture classes for the Little Washita River Basin.

TABLE 15.1
Bulk Density (Pb) (g/cm³) and Saturated Hydraulic Conductivity (K_{sat}) (cm/hr) for 5-, 15-, 30-, 50- and 70-cm Soil Depths for the LWRB

Depth (cm)	Site 1-Apache		Site 2- Berg		Site 3- DOE-EF26		Site 4- NOAA	
	P_b	K_{sat}	P_b	K_{sat}	P_b	K_{sat}	P_b	K_{sat}
5	1.52	61.26	1.60	0.22	1.52	8.54	1.56	0.48
15	1.60	12.37	1.59	0.93	1.51	1.41	1.52	0.18
30	1.50	1.92	1.48	0.01	1.59	0.38	1.56	1.06
50	1.53	0.89	1.28	64.80	1.71	0.01	1.64	0.09
70	1.61	0.03	1.49	5.28	1.73	0.01	1.67	0.06

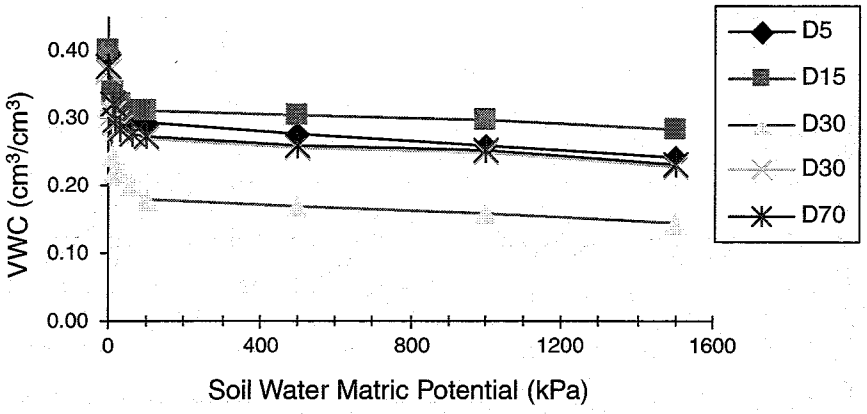

FIGURE 15.4 (See color insert following page 144.) Volumetric water content (cm^3/cm^3) for 5-, 15-, 30-, 50-, and 70-cm soil depths for NOAA site in the LWRB.

density in general increased with depth. Saturated hydraulic conductivity (K_{sat}) in general decreased with depth for all locations except the Berg site. The upper 5 and 15 cm soil depths indicated higher spatial variability of K_{sat}. Differences due to soil type and pore size distribution caused the volumetric water content to vary under different soil depths (Figure 15.4) and vegetation cover (data not shown). The temporal variations of soil moisture decreased with depth as the soil dries down (Figure 15.5). A gradual drying is observed at the deeper layers through the experimental period.

Figure 15.6 shows the temporal behavior of basin-mean, near-surface (0 to 5 cm) fractional water content (FWC) estimated at hourly time steps by SHEELS. This quantity is the proportion of saturation and is defined as volumetric water content (VWC) divided by soil porosity. From the beginning of the period until day 191, there was a general drying trend, interrupted by four minor rain events. On days 191 to 192, a substantial basin-wide rain event occurred, with a basin mean rainfall of 48 mm. This resulted in the wettest observed conditions with much of the watershed, especially the western end, briefly reaching saturation.

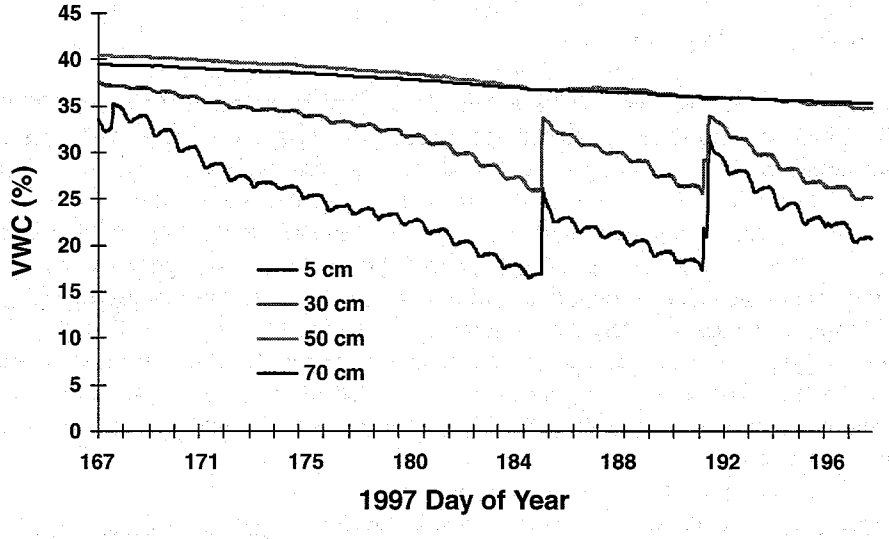

FIGURE 15.5 (See color insert following page 144.) Temporal variability of volumetric water content (%) for 5-, 30-, 50-, and 70-cm soil depths for NOAA site in the LWRB.

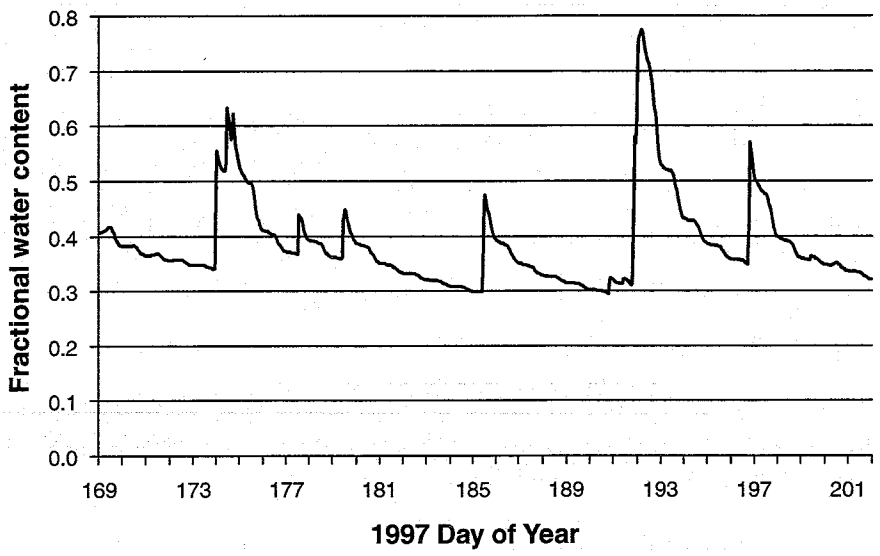

FIGURE 15.6 Basin-mean fractional soil water content estimated by SHEELS for the 0- to 5-cm layer, for each hour during the study period.

VII. DISAGGNET TRAINING

As discussed previously, our approach was to train DisaggNet, using soil water content and emissivity output from the coupled SHEELS/RTM model. Thus, the DisaggNet learns "mapping" from low (sensor) resolution ε to high (model) resolution soil water content that is conservative in ε at the footprint scale and seeks to replicate the model patterns of soil water content at each time step. Use of ε instead of T_B as input eliminates the diurnal cycle caused by surface temperature variations. The accuracy of this relationship depends on how well the SHEELS/RTM characterizes these subpixel scale patterns, i.e., the validity of our first assumption. Once DisaggNet is trained, this mapping can be applied to actual remotely sensed observations. Because the mapping preserves the pixel-scale means, any large-scale errors in the model estimates will be "corrected" via application of DisaggNet, based on our second assumption that the remotely sensed measurements are unbiased with respect to ground truth.

Model outputs used to train and validate DisaggNet were generated by running SHEELS/RTM at an hourly time step over the LWRB for the 33-day study period beginning at 0:00 UTC on day 169. Initial soil moisture conditions were specified using the ESTAR estimates from day 169. The model produces, among other variables, fractional soil water content, T_B and skin temperature at each model time step on the 800-m model grid. L-band emissivity was calculated by dividing T_B by skin temperature and then aggregated to various resolutions by averaging over 2×2, 4×4, 8×8, 16×16 and 32×32 800-m grid cells. An independent normal random deviate with zero mean and a standard deviation of 0.02 was added to each aggregated emissivity value to represent actual remotely sensed microwave observations more realistically. The emissivity standard error of 0.02 corresponds to a standard error in T_B of 6 K for a skin temperature of 300 K and was chosen to approximate errors expected from future satellite-borne microwave remote sensors. An emissivity error of 0.02 corresponds to an error of approximately 2% in volumetric water content.

DisaggNet was trained to predict high-resolution SHEELS upper zone (0 to 5 cm) FWC using approximately one-half of the study period (350 consecutive hours from days 179 through 193) over all pixels simultaneously. Training was performed separately for each emissivity aggregation (2×2 pixels, 4×4, etc.) using the following inputs:

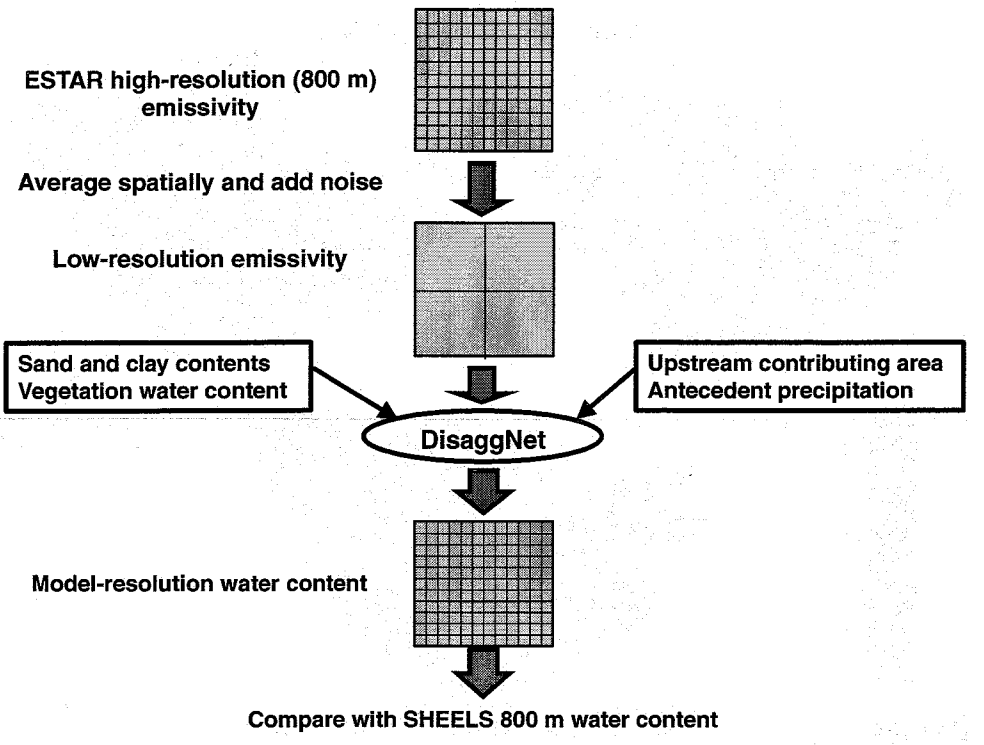

FIGURE 15.7 (See color insert following page 144.) Schematic illustrating the procedure used to apply DisaggNet.

- Remotely sensed (low-resolution) emissivity with noise
- Antecedent precipitation for the following time periods (in hours) prior to current time: 0 to 1, 1 to 3, 3 to 6, 6 to 12, 12 to 24, 24 to 48, 48 to 96 and 96 to 192
- Clay content
- Sand content
- Vegetation water content
- Upstream contributing area (surface area draining into a grid cell)

Once trained, DisaggNet generalizes for times outside the training period according to the procedure illustrated in Figure 15.7. Outputs from DisaggNet are estimates of FWC on the model grid.

VIII. VALIDATION OF DISAGGNET SOIL MOISTURE ESTIMATION

At each model time step, the trained DisaggNet generates estimates of fractional soil water content at each grid cell using the inputs listed above. Two points in time were selected to demonstrate the performance of DisaggNet. These times fall within the period used to train DisaggNet, so this is not an independent test; however, they were selected because they are close to the driest and wettest times in the study period. Output from DisaggNet for two input resolutions (2×2, or 1.6 km, and 16×16, or 12.8 km) is compared with SHEELS FWC estimates for these two times in Figures 15.8 and 15.9. As shown in Figure 15.8 for dry soil conditions at 1400 UTC on day 184, the large-scale SHEELS soil moisture pattern is captured by DisaggNet using 1.6 or 12.8 km input. This is not unexpected because the input emissivities are derived from the SHEELS soil water content via the RTM. If the emissivity–soil moisture relationship learned by DisaggNet is consistent with the relationship in the RTM, agreement should be excellent, at least when the emissivity input is not

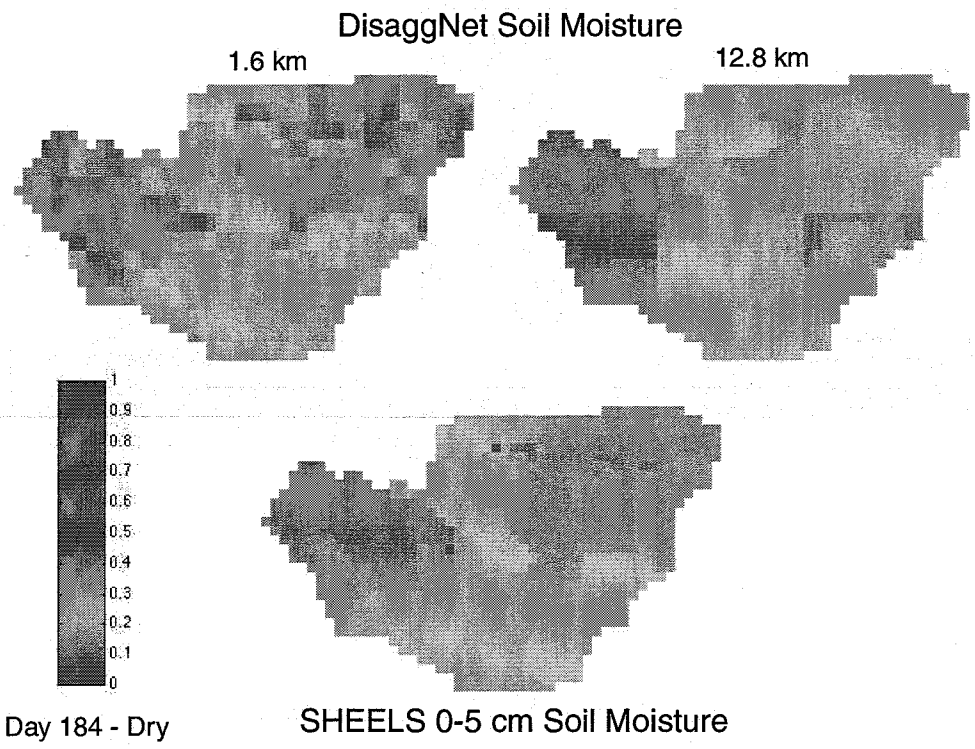

FIGURE 15.8 (See color insert following page 144.) DisaggNet soil moisture estimates for the dry soil case (1997, day 184) for 1.6 km (top left) and 12.8 km (top right) aggregated emissivity input, compared to SHEELS 0- to 5-cm soil moisture (bottom).

highly aggregated. The sources of differences between FWC estimated by DisaggNet and SHEELS are (1) aggregation of emissivity, (2) random noise added to the emissivity, and (3) inherent error associated with the neural network. In both DisaggNet output maps, the random noise is evident at the respective scale, superimposed on the overall soil moisture pattern.

The wet case corresponds to 1400 UTC on day 192 and is shown in Figure 15.9. The overall pattern is again well simulated, particularly for the high-resolution (1.6 km) case. For the low-resolution (12.8 km) case, the saturated soil in the western part of the domain is slightly underestimated. However, in the eastern half of the basin, the small-scale areas of relatively dry and wet soils are captured nicely in both cases. For example, the area of lower soil moisture associated with sandy soil in the north central part of the basin is clearly indicated by DisaggNet.

A quantitative evaluation of the agreement between soil moisture estimated by DisaggNet and by SHEELS is shown in Figures 15.10a and 15.10b in the form of root-mean-square differences (RMSD) across the LWRB at each model time step (hour). Outside of the very wet periods, RMS differences for the 1.6 and 12.8 km resolutions tend to be between 0.03 and 0.07 (3 to 7% FWC, or 1.5 to 3.5% VWC). However, during and immediately following rain periods, errors are quite large — typically greater than 0.07 (3.5% VWC) and occasionally above 0.08 (4% VWC) for the 1.6-km case and above 0.12 (6.0% VWC) for the 12.8-km case. RMS differences are slightly higher for the 12.8-km case than for the 1.6-km case, with mean values of 0.0569 and 0.0527, respectively. Table 15.2 lists the overall RMS errors for all resolutions, with and without random noise in the input emissivities.

The spatial distribution of DisaggNet-SHEELS root-mean-square differences in FWC, averaged over the 3-day study period, is shown in Figure 15.11 for the low-resolution case. RMS differences are slightly higher in the western part of the basin, where rainfall was greater, but are less than 0.1

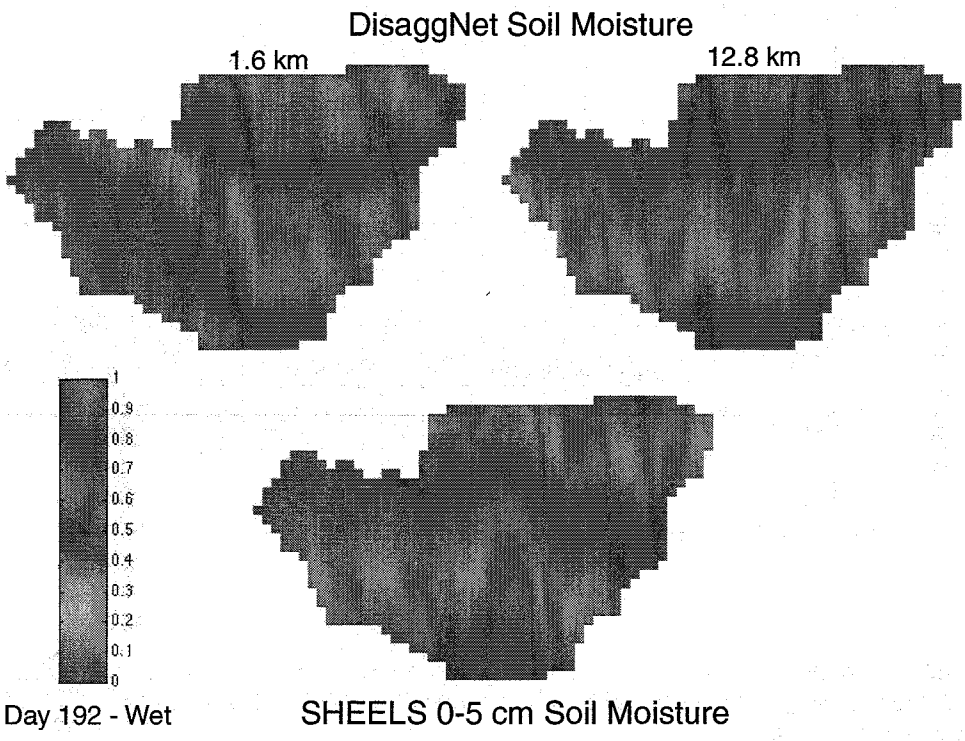

FIGURE 15.9 (See color insert following page 144.) Same as Figure 15.8 except for the wet soil case (1997, day 192).

TABLE 15.2
RMS Differences between Fractional Water Content Estimated by SHEELS and by DisaggNet, with and without Random Noise in the Emissivity Inputs, for Each Level of Emissivity Input Aggregation

Aggregation level	RMS without emissivity noise	RMS with emissivity noise
1 × 1 (0.8 km)	0.0266	0.0475
2 × 2 (1.6 km)	0.0396	0.0527
4 × 4 (3.2 km)	0.0437	0.0545
8 × 8 (6.4 km)	0.0473	0.0560
16 × 16 (12.8 km)	0.0493	0.0569
32 × 32 (25.6 km)	0.0542	0.0598

for almost the entire basin. The two points shown as having very high RMSD are, in fact, classified as water bodies in SHEELS, where the soil is treated as always saturated. This condition is not well simulated because the radiative transfer model is not configured to estimate emissivity from water surfaces properly; therefore the emissivities supplied to DisaggNet are inconsistent with the permanently saturated conditions at these grid points in SHEELS. The spatial distribution of RMSD is very similar for the high-resolution case.

The agreement between DisaggNet- and SHEELS-estimated FWC is shown in Figures 15.12a and 15.12b for the high- and low-resolution cases, for each hour during the 3-day study period, produced using noisy emissivity inputs. There is slightly more scatter in the low-resolution case, consistent with the slightly higher RMS value. Versions of the scatter plots smoothed by binning

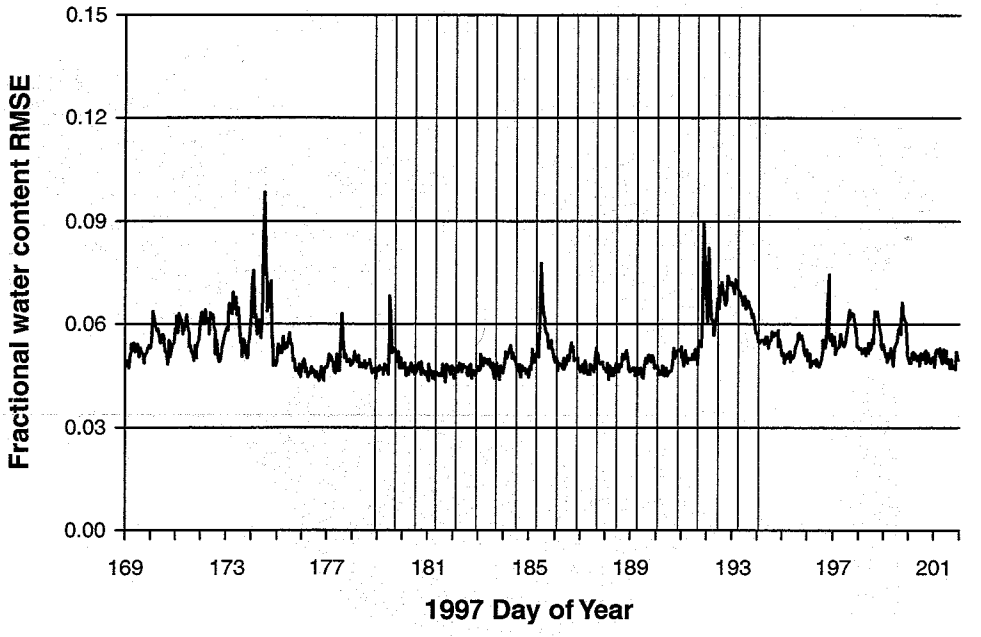

FIGURE 15.10A Root-mean-square difference time series between fractional water content estimated by SHEELS and by DisaggNet using emissivity input aggregated to 1.6-km grid cells. The time period used for DisaggNet training is shaded.

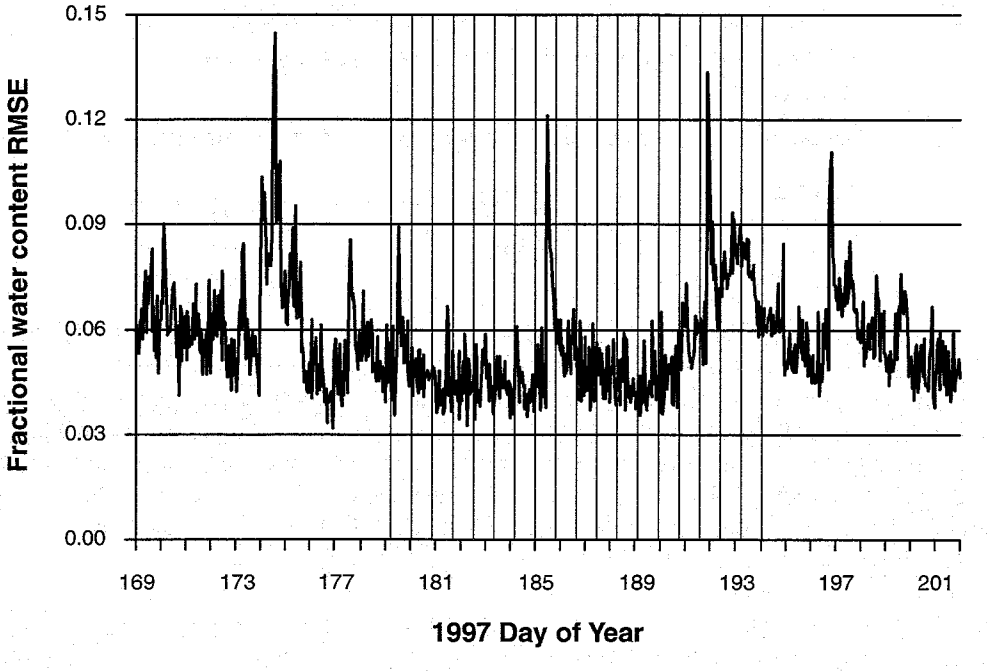

FIGURE 15.10B Same as Figure 15.10a except for 12.8 km emissivity input.

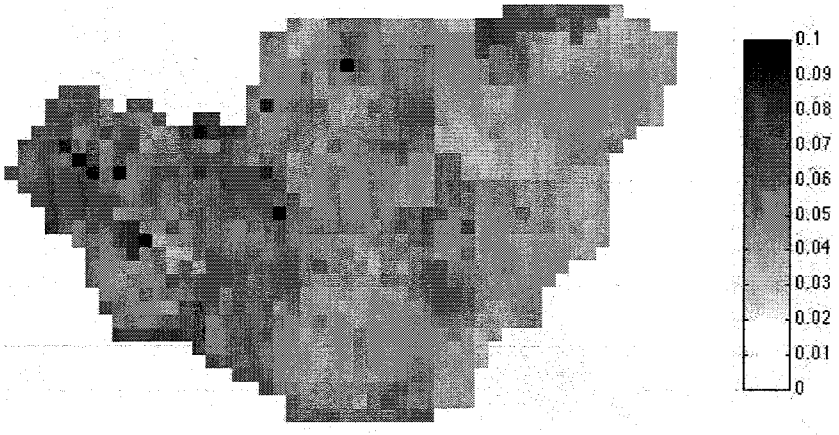

FIGURE 15.11 (See color insert following page 144.) Root-mean-square differences, averaged over the 3-day study period, between fractional water content estimated by SHEELS and by DisaggNet using inputs aggregated to 12.8-km grid cells.

FWC values are shown in Figures 15.13a and 15.13b to show better any systematic biases between DisaggNet and SHEELS estimates. In both cases, for low to moderate soil moisture conditions, DisaggNet estimates are unbiased with respect to SHEELS. At higher moisture levels (above 0.5 (0.6) for the low (high) resolution case), DisaggNet estimates become negatively biased. This is particularly pronounced for SHEELS FWC values around 0.8 and above 0.9. This result is not yet understood, but we speculate that it is due to nonlinear rainfall–FWC relationships associated with heavy rainfall that are not handled properly in DisaggNet due to its linear weighting functions. A second possible explanation is the spatial extent of saturated areas. As the input resolution becomes coarser, input emissivities are averaged, making extremely high DisaggNet estimates of FWC less likely.

IX. CONCLUSIONS

A neural-network based scheme called DisaggNet has been developed for disaggregating low-resolution satellite microwave remote sensing data to higher resolutions compatible with hydrologic data requirements. DisaggNet has been trained using output from a coupled hydrologic–radiative transfer model using input data from the SGP '97 field experiment. Results shown here focus on the driest and wettest days for the study period.

In this procedure, microwave emissivity was simulated by the coupled model and used as input to train the disaggregation scheme. Emissivity data were degraded to various resolutions by simple averaging from the model resolution of 800 m, and random Gaussian noise was added. Results are shown here for the cases using 1.6-km data (2×2 pixel averaging) and 12.8-km data (16×16 averaging). As expected, RMS differences between DisaggNet and model-simulated soil water content increased with aggregation level. RMS differences are quite low during dry periods, but somewhat larger under very wet conditions. We believe that this is due to an underestimation of high soil moisture values following heavy rainfall, due to spatial averaging of inputs or the linear nature of the rainfall–soil moisture relationship inherent in DisaggNet. Future refinements to DisaggNet will focus on modifying these linear mapping functions.

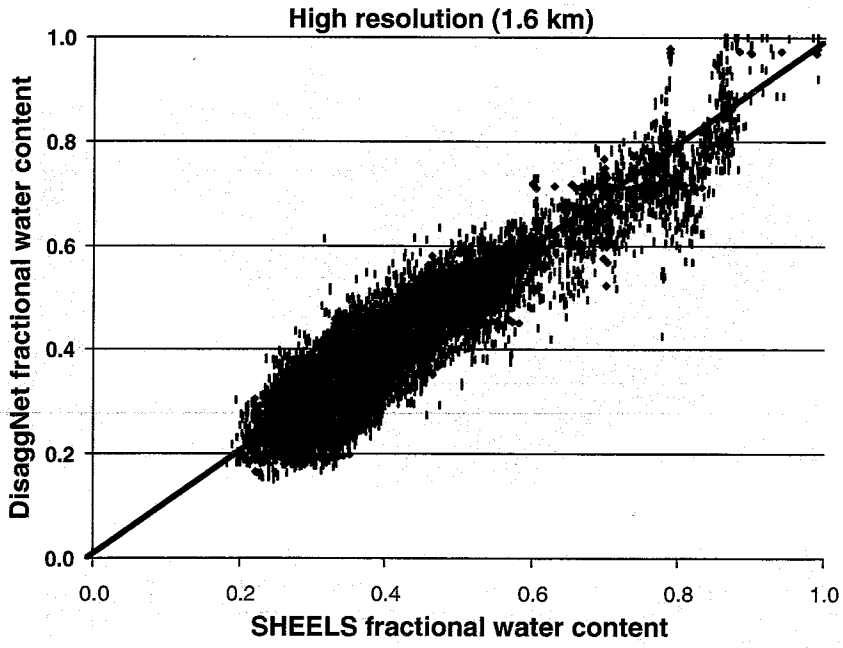

FIGURE 15.12A Scatter diagram between fractional water content estimated by SHEELS and by DisaggNet using emissivity input aggregated to 1.6-km grid cells.

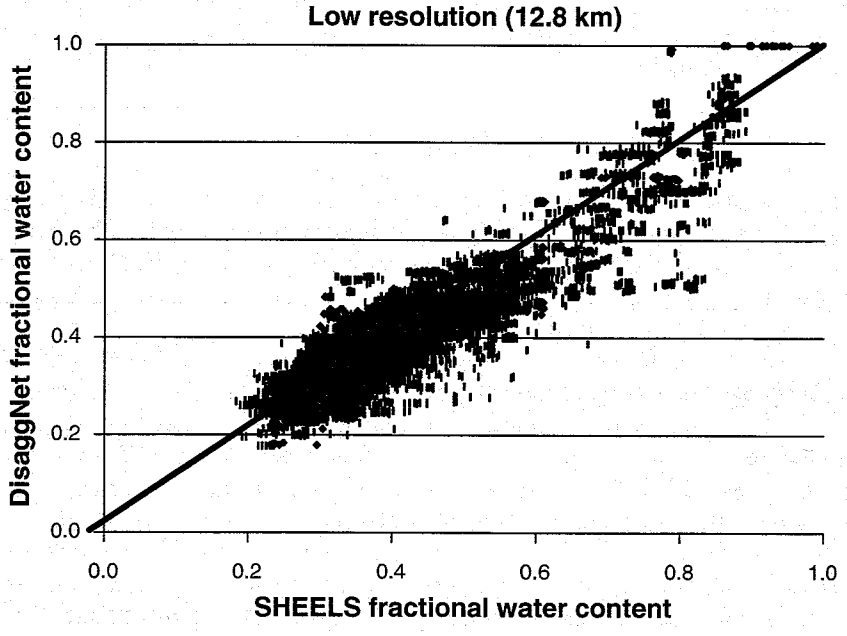

FIGURE 15.12B Same as Figure 15.12a except for 12.8 km emissivity input.

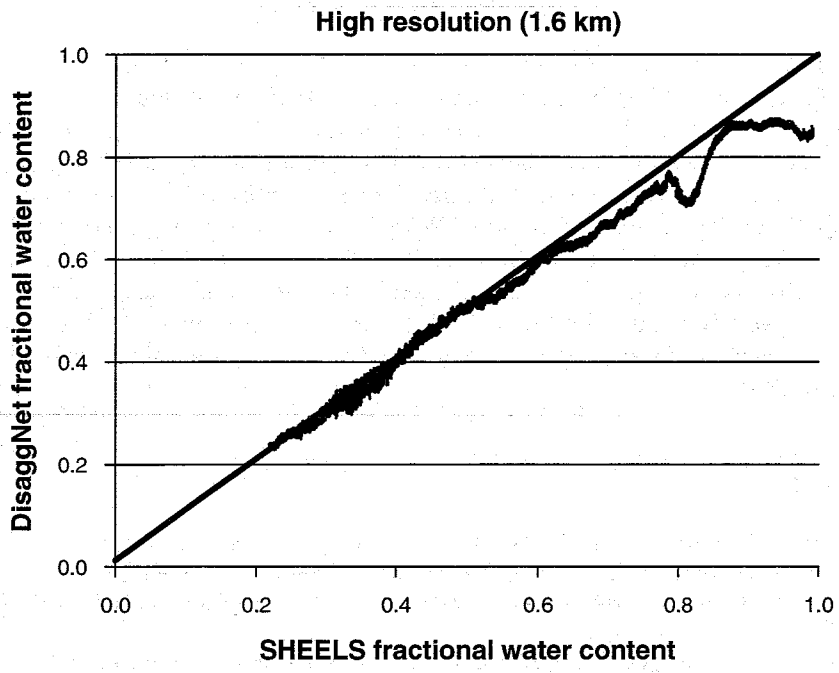

FIGURE 15.13A Smoothed scatter diagram between fractional water content estimated by SHEELS and by DisaggNet using emissivity input aggregated to 1.6-km grid cells.

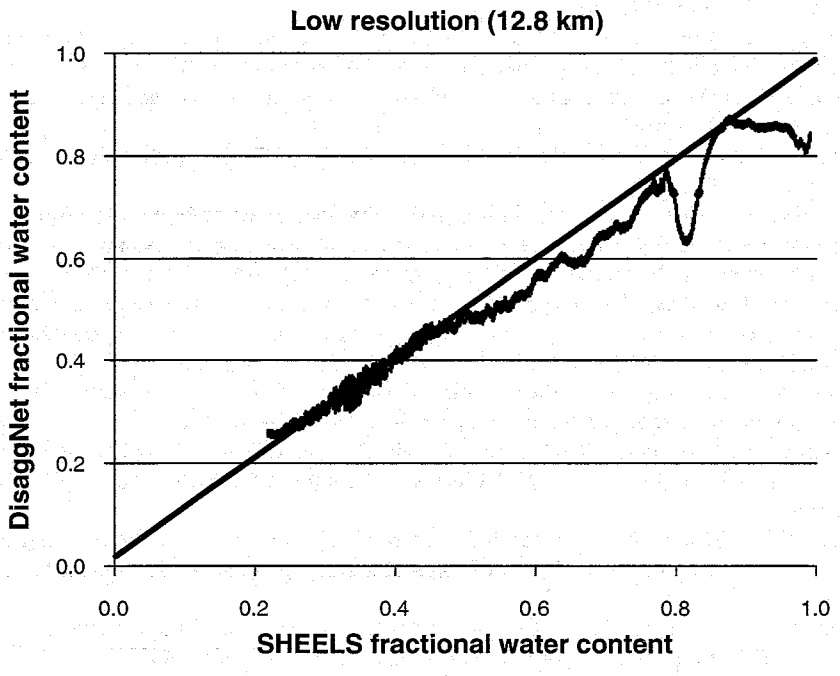

FIGURE 15.13B Same as Figure 15.13a except for 12.8 km emissivity input.

X. ACKNOWLEDGMENTS

We acknowledge Frank Archer, Ahmed Fahsi, Andrew Manu, Jimmy Moore, Narayan Rajbhandari, Garland Robertson, Vishwas Soman, and Wubishet Tadesse for their assistance during the field experiment. We thank Ashutosh Limaye for providing the gridded rainfall data product. Data were obtained from the Atmospheric Radiation Measurement (ARM) Program sponsored by the U.S. Department of Energy, Office of Energy Research, Office of Health and Environmental Research, Environmental Sciences Division. LWRB Micronet meteorological data were obtained from the USDA Agricultural Research Service. Department of Plant and Soil Sciences, Alabama A&M University, Normal, AL 35762. Contributed by the Agricultural Experiment Station, Alabama A&M University, manuscript No. 483. This work was supported by NASA Grant NCCW-0084 with Alabama A&M University's Center for Hydrology, Soil Climatology and Remote Sensing (HSCaRS).

REFERENCES

1. Engman, E.T., Angus, G., and Kustas, W.P. Relationship between the hydrologic balance of a small watershed and remotely sensed soil moisture. Remote sensing and large-scale global processes, In: *Proc. IAHS 3rd Int. Assembly*, Baltimore, MD, May, 1989. IAHS Publ. No. 186, IAHS, Wallingford, 75–84, 1989.
2. Jackson, T.J., Schmugge, T.J., and Wang, J.R. Passive microwave sensing of soil moisture under vegetation canopies, *Water Resour. Res.*, 18, 1137–1142, 1982.
3. O'Neill, P.E., Chauhan, N.S., and Jackson, T.J. Use of active and passive microwave remote sensing for soil moisture estimation through corn, *Int. J. Remote Sensing*, 17, 1851–1865, 1996.
4. Schmugge, T.J., Jackson, T.J., and McKim, H.L. Survey of methods for soil moisture determination, *Water Resour. Res.*, 16, 961–970. 1980.
5. Schmugge, T.J., O'Neill, P.E., and Wang, J. R. Passive microwave soil moisture research, *IEEE Trans. Geosci. Rem. Sens*, 14, 12–22, 1986.
6. Tsegaye, T. and Hill, R.L. Intensive tillage effects on spatial variability of soil physical properties, *Soil Sci. J.* 163:143–154,1998.
7. Tsegaye, T.D., Coleman, T.L., Crosson, W.L., Manu, A., and Boggs, J. L. Surface and subsurface characterization of soil physical properties for hydrology models, in *Agron, Abstract.* 184, 1998.
8. Tsegaye, T., Coleman, T.L., Senwo, Z.N., Tadesse, W., Rajbhandari, N.B, and Surrency, J. A. Southern Great Plains '97 Hydrology Experiment: the spatial and temporal distribution of soil moisture within a quarter section pasture field, Preprint *NASA-URC Technical Conference* Huntsville, AL,76–82,1998.
9. Tsegaye, T.D., Coleman, T.L., Manu, A., Senwo, Z., Fahsi, A., Belisle, W., Tedesse, W., Robertson, G., Boggs, J., Archer, F., Surrency, J., Birgan, L., Laymon, C., Crosson, W., and Miller, J. The spatial and temporal variability of soil moisture with and without cover crop and its impact on remote sensing, *13th Conference on Hydrology, American Meteorological Society*, 349–351, 1997.
10. Allen, P.B. and Naney, J.W. Hydrology of the Little Washita river watershed, Oklahoma: data and analyses, *Rep. ARS-90*, U.S. Dept. of Agriculture., Agric. Res. Serv., Washington, D.C., 1991.
11. Darcy, H. *Les Fontaines Publiques de la Ville de Dijon*, Dalmont, Paris. 1856.
12. Blake, G.R. and Hartge, K.H. Bulk density: In *Methods of Soil Analysis*, Part 1, 2nd ed.,A. Klute (Ed.), Agronomy monograph no. 9, ASA, Madison, WI, 363–375, 1986.
13. Dickinson, R.E., Henderson-Sellers, A., Kennedy, P.J., and Giorgi, F. Biosphere atmosphere transfer scheme (BATS) version 1e as coupled to the NCAR community climate model, *NCAR/TN-387+STR*, 72, 1993.
14. Smith, E.A., Crosson, W.L., Cooper, H.J., and Weng, H.-Y. Estimation of surface heat and moisture fluxes over a prairie grassland. Part III: Design of a hybrid physical/remote sensing biosphere model, *J. Geophys. Res.*, 98, 4951–4978,1993
15. Crosson, W.L., Laymon, C.A., Inguva, R., and Schamschula, M. Assimilating remote sensing data in a surface flux-soil moisture model, *Hydrological Processes*, 16, 1645, 2002.

16. Njoku, E.G. and Kong, N.-A. Theory for passive microwave remote sensing of near-surface soil moisture, *J. Geophys. Res.*, 82, 3108–3118, 1977.
17. Choudhury, B.J., Schmugge, T.J., Chang, A., and Newton, R.W. Effect of surface roughness on the microwave emission from soils, *J. Geophys. Res.*, 84, 5699–5706, 1979.
18. Jackson, T.J. and Schmugge, T.J. Vegetation effects on the microwave emission of soils, *Rem. Sens. Environ.*, 36, 203–212, 1991.
19. Crosson, W.L., Laymon, C.A., Inguva, R., and Bowman, C. Comparison of two microwave radiobrightness models and validation with field measurements, *IEEE Trans. Geosci. and Rem. Sens.*, 40, 143–152, 2002.
20. Jackson, T.J., LeVine, D.M., Hsu, A.Y., Oldak, A., Starks, P.J., Swift, C.T., Isham, J.D., and Haken, M. Soil moisture mapping at regional scales using microwave radiometry: the Southern Great Plains Hydrology Experiment, *IEEE Trans. Geosci. Rem. Sens.*, 37, 2136–2151, 1999.

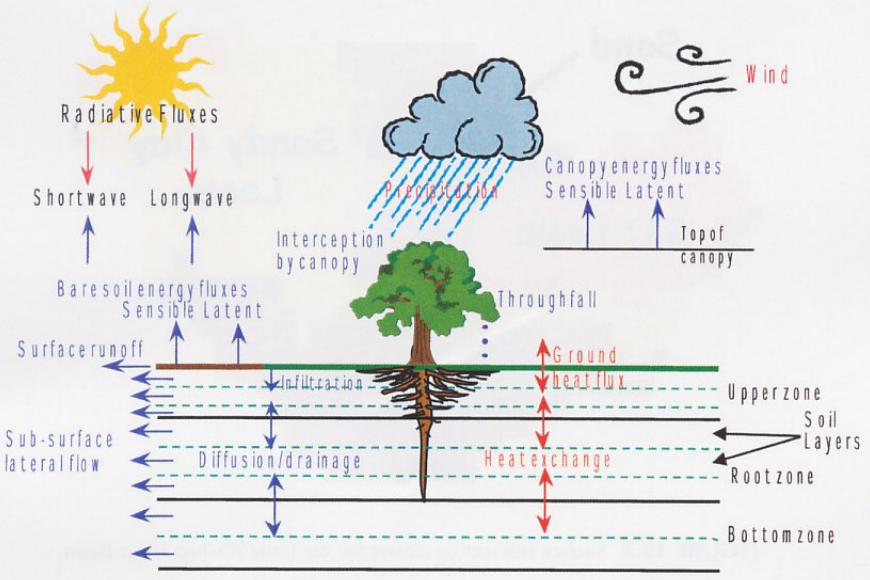

FIGURE 15.1 Schematic representation of the basic energy flux and hydrologic processes in the simulator for hydrology and energy exchange at the land surface (SHEELS).

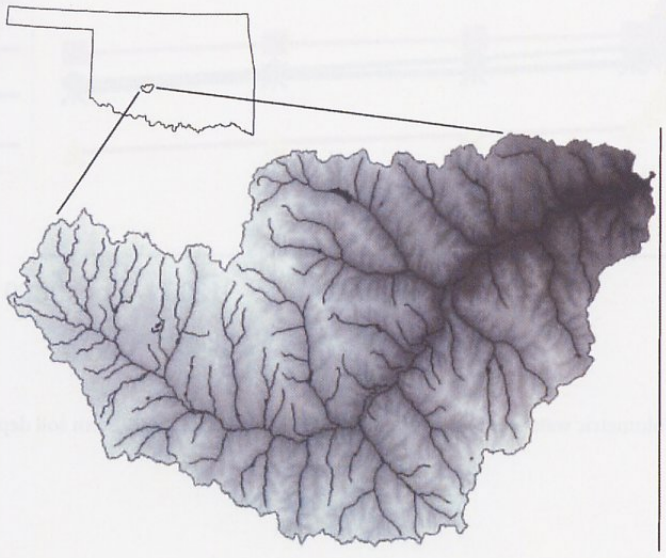

FIGURE 15.2 Digital elevation model and stream network for the Little Washita River Basin, Oklahoma.

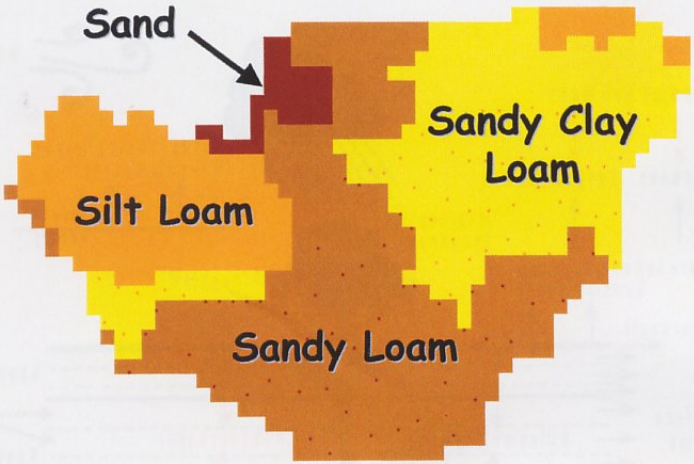

FIGURE 15.3 Surface soil texture classes for the Little Washita River Basin.

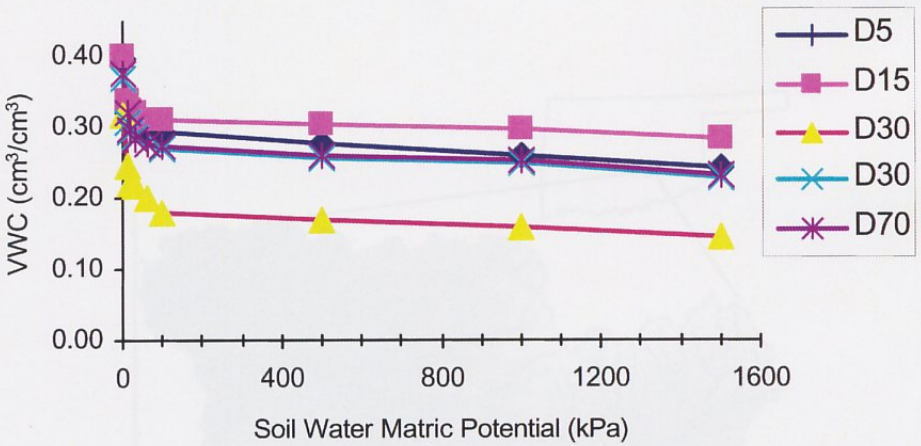

FIGURE 15.4 Volumetric water content (cm^3/cm^3) for 5-, 15-, 30-, 50-, and 70-cm soil depths for NOAA site in the LWRB.

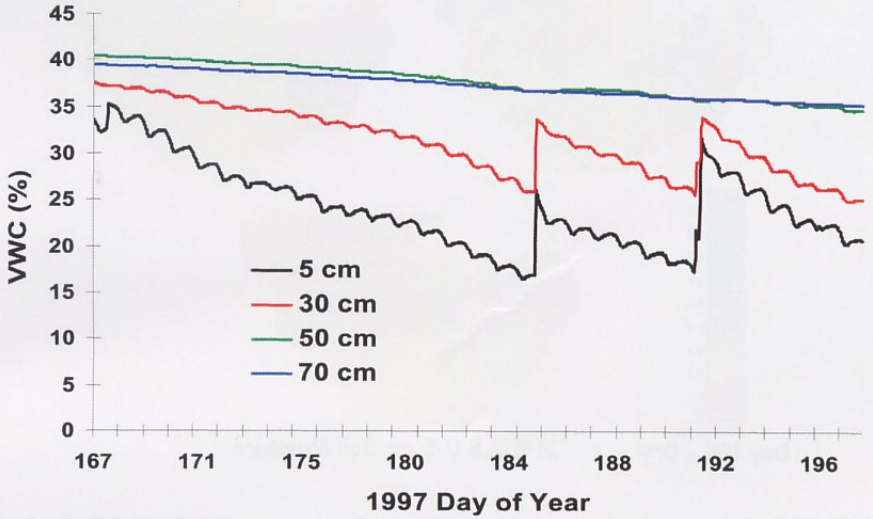

FIGURE 15.5 Temporal variability of volumetric water content (%) for 5-, 30-, 50-, and 70-cm soil depths for NOAA site in the LWRB.

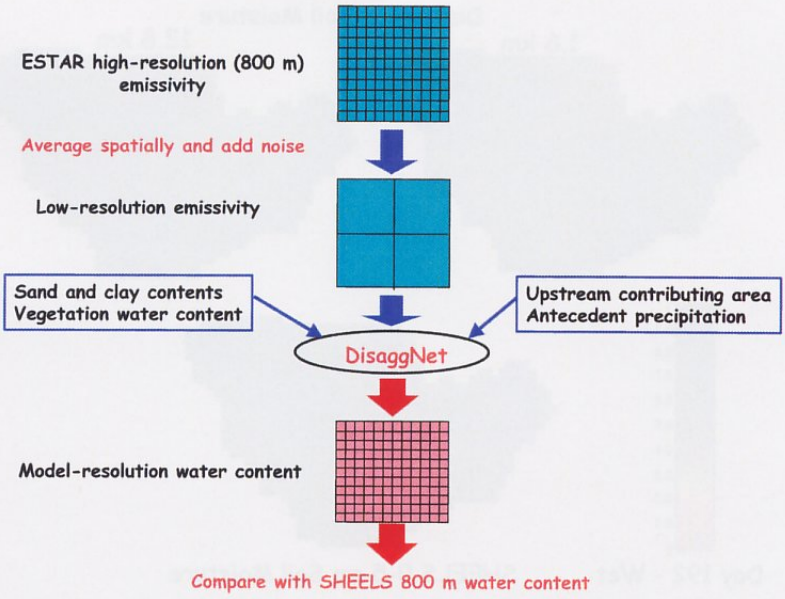

FIGURE 15.7 Schematic illustrating the procedure used to apply DisaggNet.

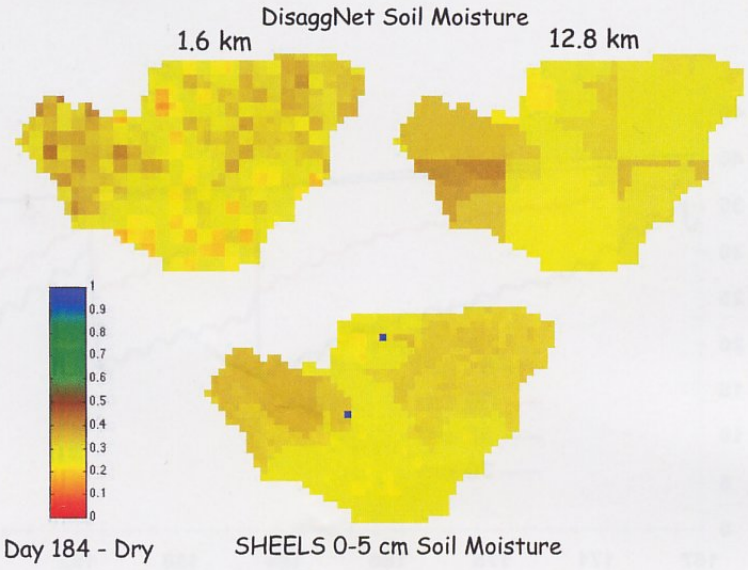

FIGURE 15.8 DisaggNet soil moisture estimates for the dry soil case (1997, day 184) for 1.6 km (top left) and 12.8 km (top right) aggregated emissivity input, compared to SHEELS 0- to 5-cm soil moisture (bottom).

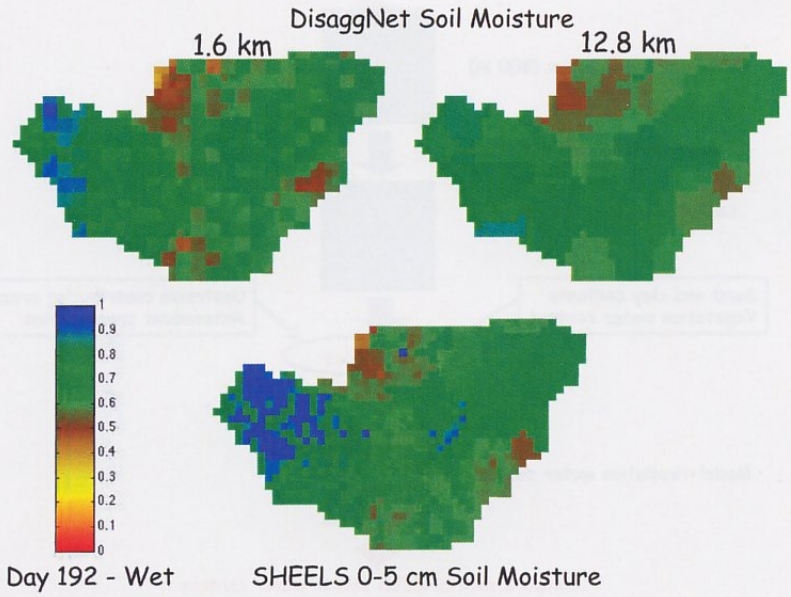

FIGURE 15.9 Same as Figure 15.8 except for the wet soil case (1997, day 192).